

Unusual Contact Shifts and Magnetic Tensor Orientation in *Rhodobacter capsulatus* Ferrocyclochrome *c'*: NMR, Magnetic Susceptibility, and EPR Studies

Pascale Tsan,^{†,‡} Michael Caffrey,^{†,||} Max Lawson Daku,[‡] Michael Cusanovich,[§] Dominique Marion,[†] and Pierre Gans^{*,†}

Contribution from the Institut de Biologie Structurale "Jean-Pierre Ebel" (CEA-CNRS), 41 Avenue des Martyrs, 38027 Grenoble Cedex, France, DRFMC-SCIB-SCPM, 85X, CEN-Grenoble, 38041 Grenoble Cedex, France, and Department of Biochemistry, University of Arizona, Tucson, Arizona 85721

Received June 15, 1998

Abstract: In contrast to high-spin ferrous paramagnetic heme proteins, the chemical shifts of the heme protons are very unusual in the ferrocyclochromes *c'*. Magnetic susceptibility studies of *Rhodobacter capsulatus* ferrocyclochrome *c'* in frozen solutions have been performed and indicate an $S = 2$ spin state and a large negative axial (D) zero-field splitting parameter (-18.3 cm^{-1}) as well as a significant rhombic (E) value (-4.9 cm^{-1}). The ^1H and ^{15}N resonances have been extensively assigned by TOCSY-HSQC, NOESY-HSQC, and HSQC-NOESY-HSQC 3-D heteronuclear experiments performed on a 8 mM sample labeled with ^{15}N . Based on short-range and medium-range NOEs and H^{N} exchange rates, the secondary structure consists of four helices: helix-1 (3–30), helix-2 (34–49), helix-3 (78–97), and helix-4 (103–117). The ^{15}N , H^{N} , and H^{α} chemical shifts of the reduced (or ferro) state are compared to those previously assigned for the diamagnetic carbon monoxide complex form. From the chemical shift differences between these redox states, the orientation and the anisotropy of the paramagnetic susceptibility tensor have been determined using the crystallographic coordinates of the ferric state. Values of -23 and -3 cm^{-1} have been inferred for D and E , and the z -axis of the tensor is tilted approximately 30° from the normal to the heme. The paramagnetic chemical shifts of the heme protons have been determined and split up into Fermi shift and the dipolar shift contributions. The pattern of the contact shifts is very unusual, exhibiting a 2-fold symmetry, and is discussed in terms of molecular orbital interactions between the porphyrin macrocycle and the imidazole ring.

Introduction

The cytochromes *c'* (Cyt c')¹ are class II cytochromes *c*, which are characterized by heme attachment to the C-terminal region of the protein, histidine as an axial ligand, and the absence of a second axial ligand.² Typically, Cyt c' are dimers made of two identical subunits, each consisting of a four-helix bundle structural motif,^{3,4} but monomeric species have also been

characterized in solution for *Rhodospseudomonas palustris*⁵ or, in the solid state, for the *Rhodobacter capsulatus* St. Louis strain.^{4c} Cyt c' present low redox potentials varying from -10 to $+100 \text{ mV}$,^{2,6} and, at present, their physiological role remains unknown. As their concentration levels in photosynthetic bacteria are regulated by the presence of light and oxygen, it has been postulated that they play some role in a metabolic pathway active during photosynthesis.^{2,7} They also occur in denitrifying nonphotosynthetic bacteria, where they might be involved in the nitrogen assimilation.^{2,6} The physiologically

* To whom correspondence should be addressed. E-mail: pierre@rmn.ibs.fr. Telephone: (33) 476885798. Fax: (33) 476885494.

[†] Institut de Biologie Structurale "Jean-Pierre Ebel".

[‡] DRFMC-SCIB-SCPM.

[§] University of Arizona.

^{||} Present address: Biological NMR Center, Medical Sciences Building, University of Leicester, Leicester LE1 7RH, U.K.

^{||} Present address: Laboratory of Chemical Physics, NIDDK/NIH, Bethesda, MD 20892.

(1) Abbreviations used: Cyt c' , cytochrome *c'*; HMQC, heteronuclear multiple-quantum coherence spectroscopy; HSQC, heteronuclear single-quantum coherence spectroscopy; NMR, nuclear magnetic resonance; NOE, nuclear Overhauser effect; NOESY, nuclear Overhauser enhancement spectroscopy; TOCSY, total correlated spectroscopy; TPPI, time-proportional phase incrementation; WATERGATE, water suppression by gradient-tailored excitation; EPR, electron paramagnetic resonance; MCD, magnetic circular dichroism; EXAFS, extended X-ray absorption fine structure; ZFS, zero-field splitting; EFG, electric field gradient; OEP, octaethylporphyrin; OETPP, octaethyltetraphenylporphyrin; 2-MeHim, 2-methylimidazole.

(2) Bartsch, R. G. In *The Photosynthetic Bacteria*; Clayton, R. K., Sistrom, W. R., Eds.; Plenum: New York, 1978; pp 249–280. Meyer, T.; Kamen, M. *Adv. Protein Chem.* **1982**, *35*, 105–212. Pettigrew, G. W.; Moore, G. R. *Cytochromes c: Biological aspects*; Springer-Verlag: Berlin, 1987.

(3) Moore, G. R.; Pettigrew, G. W. *Cytochromes c: Evolutionary, Structural and Physicochemical Aspects*; Springer-Verlag: Berlin, 1990. Weber, P. C.; Howard, A.; Xuong, N. H.; Salemme, F. R. *J. Mol. Biol.* **1981**, *153*, 399–424. Finzel, B.; Weber, P. C.; Hardman, K.; Salemme, F. R. *J. Mol. Biol.* **1985**, *186*, 627–643. Yasui, M.; Harada, S.; Kai, Y.; Kasai, N.; Kusunoki, M.; Matsuura, N. *J. Biochem. (Tokyo)* **1992**, *111*, 317–324. Ren, Z.; Meyer, T.; McRee, D. *J. Mol. Biol.* **1993**, *234*, 433–445. Dobbs, A. J.; Anderson, B. F.; Faber, H. R.; Baker, E. N. *Acta Crystallogr.* **1996**, *D52*, 356–368.

(4) (a) Tahirov, T. H.; Misaki, S.; Meyer, T. E.; Cusanovich, M. A.; Higuchi, Y.; Yasuoka, N. *Nature, Struct. Biol.* **1996**, *3*, 459–464. (b) Tahirov, T. H.; Misaki, S.; Meyer, T. E.; Cusanovich, M. A.; Higuchi, Y.; Yasuoka, N. *J. Mol. Biol.* **1996**, *259*, 467–479. (c) Tahirov, T. H.; Misaki, S.; Meyer, T. E.; Cusanovich, M. A.; Higuchi, Y.; Yasuoka, N. *Acta Crystallogr.* **1997**, *D53*, 658–664.

(5) Cusanovich, M. A. *Biochim. Biophys. Acta* **1970**, *236*, 238–241.

(6) Yamanaka, T. *The Biochemistry of Bacterial Cytochromes*; Japan Scientific Societies Press: Tokyo, 1992; pp 89–168.

(7) Cusanovich, M. A.; Bartsch, R. G.; Kamen, M. D. *Biochim. Biophys. Acta* **1968**, *153*, 397–417. Morita, S. *Biochim. Biophys. Acta* **1968**, *153*, 241–247.

relevant state of Cyt c' is considered to be the reduced state, as the characteristic EPR spectrum of ferriCyt c' has not been detected in vivo.⁸ On the other hand, although purified ferriCyt c' binds CO, intact cells do not bind the CO which would be expected from their Cyt c' content.⁷ As compared to other hemoproteins, the magnetic properties of Cyt c' are unique. In most species, the heme Fe has been described as a quantum mechanical admixture of high and intermediate spins ($S = 5/2$ and $3/2$) in the oxidized (or ferric) state.⁹ For this reason, ferriCyt c' have been widely characterized by NMR,¹⁰ EPR,¹¹ Mössbauer spectroscopy,¹² MCD,¹³ resonance Raman,¹⁴ and EXAFS spectroscopy.¹⁵ In contrast, only a few studies have been devoted to the magnetic properties of the reduced ferrous state, despite its physiological interest. In this state, the heme Fe is high spin ($S = 2$), as indicated by Mössbauer spectroscopy^{12a} and magnetic susceptibility measurements at room temperature,^{10a} and pentacoordinate, as inferred from resonance Raman,¹⁴ MCD,¹³ and EXAFS data.¹⁵ These iron properties are analogous to those observed by Mössbauer, EPR, or magnetic susceptibility studies for deoxymyoglobins^{16,17} or deoxyhemoglobins.¹⁷ However, the pattern of the paramagnetic shifts of the four methyl protons is reversed in the Cyt c' with respect to those of myoglobins,^{16,17} hemoglobins,¹⁷ and model compounds such as microperoxidase-11¹⁸ or iron(II) porphyrins.¹⁹ NMR studies have essentially focused on the assignment of the paramagnetic heme

protons, but no characterization of the contact shifts has been performed.^{10a,e,f} Moreover, ferroCyt c' , in contrast to myoglobin or hemoglobin, present a splitting of the Soret band, which is interpreted as a d-type hyperporphyrin spectrum resulting from a charge transfer between occupied π -orbitals of the macrocycle to the e_g orbital of the iron in a highly asymmetric heme environment.²⁰ This has led us to fully characterize the reduced state of a Cyt c' in order to understand the structural and/or magnetic properties at the basis of this unusual chemical shift pattern.

In paramagnetic proteins, the observed chemical shift is described by

$$\delta_{\text{obs}} = \delta_{\text{dm}} + \delta_{\text{pm}} \quad (1)$$

where δ_{obs} , δ_{dm} , and δ_{pm} are the observed, diamagnetic, and paramagnetic (or hyperfine) shifts, respectively. The paramagnetic shift arises from two contributions, the Fermi contact due to spin density delocalization along chemical bonds and the dipolar shift linked to the electron dipolar field.²¹ For nuclei not scalar coupled to the paramagnetic center, δ_{pm} reduces to the dipolar (or pseudocontact) effect and is described by the general equation²¹

$$\delta_{\text{pm}} = (1/2r^3)\{^{2/3}(3 \cos^2 \theta - 1)(\chi_{zz} - 1/2(\chi_{xx} + \chi_{yy})) + (\sin^2 \theta \cos 2\phi)(\chi_{xx} - \chi_{yy})\} \quad (2)$$

where χ_{xx} , χ_{yy} , and χ_{zz} are the principal components of the magnetic susceptibility tensor and r , θ , and ϕ are the polar coordinates of the nucleus in the reference frame defined by the principal axes of the χ -tensor with the origin at the electronic density center.

Thus, provided the protein structure, from which the geometric factors r , θ , and ϕ can be inferred, has been independently obtained by either X-ray crystallography or NMR, the experimental determination of δ_{pm} allows one to characterize the orientation and magnitude of the magnetic susceptibility tensor and, in turn, the Fermi shift for the protons of the metal ligands. Determination of these parameters reveals information on the magnetic properties of the metal at room temperature which are difficult to determine by other techniques. Numerous NMR studies of low-spin heme proteins including cytochromes c ,^{22,23} cytochromes b ,²⁴ and cyanometmyoglobins²⁵ have shown that the chemical shift difference between the oxidized ($S = 1/2$) and reduced ($S = 0$) states can be used to derive the electronic g -tensor and detect structural differences between the redox states.

(20) Yoshimura, T.; Suzuki, S.; Nakahara, A.; Iwasaki, H.; Masuko, M.; Matsubara, T. *Biochim. Biophys. Acta* **1985**, *831*, 267–274.

(21) Jesson, J. P. In *NMR of Paramagnetic Molecules. Principles and Applications*; La Mar, G. N., Horrocks, W. DeW., Jr., Holm, R. H., Eds.; Academic Press: New York, 1973; pp 2–52.

(22) Williams, G.; Clayden, N. J.; Moore, G. R.; Williams, R. J. P. *J. Mol. Biol.* **1985**, *183*, 447–460. Trewhella, J.; Carlson, V.; Curtis, E.; Heidorn, D. *Biochemistry* **1988**, *27*, 1121–1125. Gao, Y.; Boyd, J.; Pielak, G. J.; Williams, R. J. P. *Biochemistry* **1991**, *30*, 1928–1934. Gao, Y.; Boyd, J.; Pielak, G. J.; Williams, R. J. P. *Biochemistry* **1991**, *30*, 7033–7040. Timkovich, R.; Cai, M. *Biochemistry* **1993**, *32*, 11516–11523. Turner, D. L.; Williams, R. J. P. *Eur. J. Biochem.* **1993**, *211*, 555–562. Zhao, D.; Hutton, H. M.; Cusanovich, M. A.; MacKensie, N. E. *Protein Sci.* **1996**, *5*, 1816–1825.

(23) Feng, Y.; Roder, H.; Englander, S. *Biochemistry* **1990**, *29*, 3494–3504.

(24) (a) Veitch, N. C.; Whitford, D.; Williams, R. J. P. *FEBS Lett.* **1990**, *269*, 297–304. (b) Guiles, R. D.; Basus, V. J.; Sarma, S.; Malpure, S.; Fox, K. M.; Kuntz, I. D.; Waskell, L. *Biochemistry* **1993**, *32*, 8329–8340.

(25) Emerson, S. D.; La Mar, G. N. *Biochemistry* **1990**, *29*, 1556–1566. Banci, L.; Pierattelli, R.; Turner, D. L. *Eur. J. Biochem.* **1995**, *232*, 522–527.

(8) Dutton, P. L.; Leigh, J. S. *Biochim. Biophys. Acta* **1973**, *314*, 178–190.; Prince, R. C.; Leigh, J. S.; Dutton, P. L. *Biochem. Soc. Trans.* **1974**, *2*, 950–953. Corker, G. A.; Sharpe, S. A. *Photochem. Photobiol.* **1975**, *21*, 49–61. Monkara, F.; Bingham, S. J.; Kadir, F. H. A.; McEwan, A. G.; Thomson, A. J.; Thurgood, A. G. P.; Moore, G. R. *Biochim. Biophys. Acta* **1992**, *1100*, 184–188.

(9) Maltempo, M. M.; Moss, T. H. *Q. Rev. Biophys.* **1976**, *9*, 181–215.

(10) (a) Emptage, M.; Xavier, A.; Wood, J.; Alsaadi, B.; Moore, G.; Pitt, R.; Williams, R.; Ambler, R.; Bartsch, R. *Biochemistry* **1981**, *20*, 58–64. (b) Jackson, T.; La Mar, G.; Bartsch, R. *J. Biol. Chem.* **1983**, *258*, 1799–1805. (c) Akutsu, H.; Kyogoku, Y.; Horio, T. *Biochemistry* **1983**, *22*, 2055–2063. (d) La Mar, G.; Jackson, T.; Dugad, L.; Cusanovich, M.; Bartsch, R. G. *J. Biol. Chem.* **1990**, *265*, 16173–16180. (e) Banci, L.; Bertini, I.; Turano, P.; Vicens Olivier, M. *Eur. J. Biochem.* **1992**, *204*, 107–112. (f) Bertini, I.; Gori, G.; Luchinat, C.; Vila, A. *Biochemistry* **1993**, *32*, 776–783. (g) Caffrey, M.; Simorre, J.-P.; Brutscher, B.; Cusanovich, M. A.; Marion, D. *Biochemistry* **1995**, *34*, 5904–5912. (h) Caffrey, M.; Simorre, J.-P.; Cusanovich, M. A.; Marion, D. *FEBS Lett.* **1995**, *368*, 519–522. (i) Clark, K.; Dugad, L. B.; Bartsch, R. G.; Cusanovich, M. A.; La Mar, G. N. *J. Am. Chem. Soc.* **1996**, *118*, 4654–4664.

(11) Ehrenberg, A.; Kamen, M. D. *Biochim. Biophys. Acta* **1965**, *102*, 333–340. Maltempo, M. M. *J. Chem. Phys.* **1974**, *61*, 2540–2547. Fujii, S.; Yoshimura, T.; Kamada, H.; Yamaguchi, K.; Suzuki, S.; Shidara, S.; Takakuwa, S. *Biochim. Biophys. Acta* **1995**, *1251*, 161–169.

(12) (a) Moss, T. H.; Bearden, A. J.; Bartsch, R. G.; Cusanovich, M. A. *Biochemistry* **1968**, *7*, 1583–1590. (b) Emptage, M. H.; Zimmermann, R.; Que, L., Jr.; Münck, E.; Hamilton, W. D.; Orme-Johnson, W. H. *Biochim. Biophys. Acta* **1977**, *495*, 12–23.

(13) Rawlings, J.; Stephens, P. J.; Nafie, L. A.; Kamen, M. D. *Biochemistry* **1977**, *16*, 1725–1729.

(14) Strekas, T. C.; Spiro, T. G. *Biochim. Biophys. Acta* **1974**, *351*, 237–245. Kitagawa, T.; Ozaki, Y.; Kyogoku, Y.; Horio, T. *Biochim. Biophys. Acta* **1977**, *495*, 1–11. Hobbs, J. D.; Larsen, R. W.; Meyer, T. E.; Hazzard, J. H.; Cusanovich, M. A.; Ondrias, M. R. *Biochemistry* **1990**, *29*, 4166–4174. Othman, S.; Richaud, P.; Verméglio, A.; Desbois, A. *Biochemistry* **1996**, *35*, 9224–9234.

(15) Korszun, Z. R.; Bunker, G.; Khalid, S.; Scheidt, W. R.; Cusanovich, M. A.; Meyer, T. E. *Biochemistry* **1989**, *28*, 1513–1517.

(16) Bougault, C. M.; Dou, Y.; Ikeda-Saito, M.; Langry, K. C.; Smith, K. M.; La Mar, G. N. *J. Am. Chem. Soc.* **1998**, *120*, 2113–2123.

(17) (a) La Mar, G. N.; Budd, D. L.; Goff, H. *Biochem. Biophys. Res. Commun.* **1977**, *77*, 104–110. (b) La Mar, G. N.; Anderson, R. A.; Budd, D. L.; Smith, K. M.; Langry, K. C.; Gersonde, K.; Sick, H. *Biochemistry* **1981**, *20*, 4429–4436. (c) La Mar, G. N.; Davis, N. L.; Johnson, R. D.; Smith, W. S.; Hauksson, J. B.; Budd, D. L.; Dalichow, F.; Langry, K. C.; Morris, I. K.; Smith, K. M. *J. Am. Chem. Soc.* **1993**, *115*, 3869–3876.

(18) Mazumdar, S.; Mehdi, O. K.; Mitra, S. *Inorg. Chem.* **1991**, *30*, 700–705.

(19) Walker, F. A.; Simonis, U. In *Biological Resonance NMR*; Berliner, L. J., Reuben, J., Eds.; Plenum Press: New York, 1993; Vol. 12, pp 133–274.

In high-spin hemoproteins, the dipolar shift generally arises from the existence of a significant zero-field splitting, and the susceptibility values in eq 2 are given by

$$\Delta\chi_{ax} = \chi_{zz} - \frac{1}{2}(\chi_{xx} + \chi_{yy}) = -\left[\frac{S(S+1)(2S-1)(2S+3)g^2\beta^2}{30k^2T^2}\right]D \quad (3)$$

$$\Delta\chi_{rh} = (\chi_{xx} - \chi_{yy}) = -\left[\frac{S(S+1)(2S-1)(2S+3)g^2\beta^2}{30k^2T^2}\right]2E \quad (4)$$

where D and E are the axial and rhombic zero-field splitting parameters.^{21,26}

To our knowledge, very few NMR studies of high-spin ferric heme proteins have used chemical shift differences between redox states to derive D and probe for structural differences between redox states.²⁷ As the reduced state is also paramagnetic, the lack of a diamagnetic reference prevents the use of eq 1 for this purpose. As yet, such a study has not been performed for a ferriCyt c', although the observed chemical shifts of protons located in the heme cavity are in agreement, for the monomeric Cyt c' of *Rsp. palustris*, with the predicted shifts using the D value typical of high-spin iron proteins and a model built from the structure of the *Rhodospirillum molischanum* Cyt c'.¹⁰ⁱ

In the case of ferrous $S = 2$ hemoproteins, the situation is more complex, as the g -tensor is not necessarily isotropic,¹⁶ and derivation of g -tensor values or the D value from the magnetic susceptibility tensor components needs complementary studies, such as EPR or magnetic susceptibility measurements. So far, the iron magnetic properties have been characterized only on sperm whale deoxymyoglobin, and data evidence an $S = 2$ spin state and a contribution of a large zero-field splitting (ZFS) factor rather than an anisotropy of the g -tensor.¹⁶

In the present work, we have performed magnetic susceptibility experiments as a function of the temperature, which indicate that the iron(II) is in an isolated spin state over the studied range. We have extensively assigned the resonances in the reduced state of *Rb. capsulatus* Cyt c' by a combination of 3D heteronuclear experiments. We show that medium-range NOEs and H^N exchange rates are consistent with a four-helix bundle structural motif, similar to the oxidized state and the CO complex form. The 1H and ^{15}N resonances of the ferriCyt c' and the diamagnetic carbon monoxide complex form have been previously assigned,^{10g,28} and we have determined the orientation of the magnetic susceptibility tensor axes and the magnetic anisotropy from H^N , H^α , and ^{15}N chemical shift differences with the diamagnetic state. The ZFS of the reduced state has been estimated and agrees with the amplitude and the signs of the parameters determined by magnetic susceptibility measurements. The respective contributions of the Fermi contact shift and the dipolar shift have been separated and analyzed.

Materials and Methods

Protein Preparation. Preparation of ^{15}N -labeled *Rb. capsulatus* Cyt c' has been previously described.^{10g} For the assignment experiments, the sample was concentrated at 4 °C to approximately 8 mM (heme

concentration) in buffer containing 100 mM PO_4 (pH 6.0). Oxygen was removed by blowing argon gas over the solution surface for approximately 15 min. The sample was reduced by the addition of approximately 10 mg of sodium dithionite (Janssen Chimica) and sealed. Under these conditions, the sample was stable for several months. For the H^N exchange experiments, the sample was concentrated at 4 °C to approximately 2 mM (heme concentration) in buffer containing 100 mM PO_4 (pH 6.0) and lyophilized. Deoxygenated D_2O containing approximately 10 mg of sodium dithionite was added at the start of the NH exchange experiment. Completion of the reduction reaction was checked by the absence of any of the characteristic heme methyl resonances of the oxidized form between 60 and 90 ppm.¹⁰

NMR Experiments. NMR experiments were performed on Bruker AMX400 and AMX600 spectrometers equipped with 1H and ^{15}N double-resonance probes operating at a temperature of 300 K. For the 2D HSQC experiments, the spectral widths for the direct and indirect dimensions were 7 and 30 ppm, respectively. The carrier positions for 1H and ^{15}N were 8.40 and 117.4 ppm, respectively. Spectra were acquired with 160 complex points in t_1 and 16 scans per t_1 increment, for a total experimental time of 2 h. The 3D TOCSY-HSQC, NOESY-HSQC, and HSQC-NOESY-HSQC experiments were similar to the TOCSY-HMQC,²⁹ NOESY-HMQC,³⁰ and HMQC-NOESY-HMQC³¹ experiments previously described except for the following modifications: (1) a better ^{15}N resolution can be obtained with the HSQC sequence compared to that with the HMQC sequence³² and (2) pulsed field gradients³³ were added to suppress undesired coherence transfer pathways. In addition, the WATERGATE sequence³⁴ was added for solvent suppression in the TOCSY-HSQC and NOESY-HSQC experiments. For the TOCSY-HSQC and NOESY-HSQC experiments, the spectral widths for 1H , ^{15}N , and 1H were 7, 30, and 12 ppm, respectively; carrier positions for 1H , ^{15}N , and 1H were 8.40, 117.4, and 4.75 ppm, respectively. Spectra were acquired with 256 complex points in t_1 , 80 complex points in t_2 , and 8 scans per t_1/t_2 increment, resulting in a total experimental time of approximately 60 h. For the TOCSY-HSQC experiment, the isotropic mixing time was 40 ms (not including delays), and the field strength of the 1H WALTZ-16 spin lock was 12 kHz. For the HSQC-NOESY-HSQC experiment, the spectral widths for ^{15}N , ^{15}N , and 1H were 30, 30, and 7 ppm, respectively; carrier positions for ^{15}N , ^{15}N , and 1H were 117.4, 117.4, and 8.40 ppm, respectively. Spectra were acquired with 92 complex points in t_1 , 92 complex points in t_2 , and 16 scans per t_1/t_2 increment (total experimental time 60 h). For the NOESY-HSQC and HSQC-NOESY-HSQC experiments, the mixing time was 120 ms. For the ^{15}N -edited experiments, further solvent suppression was accomplished by weak presaturation (approximately $\gamma B_1 \approx 10$ Hz) during the relaxation delay of 1.2 s. The field strengths for WALTZ-16 decoupling³⁵ of 1H and ^{15}N were 2.8 and 2.1 kHz, respectively. Quadrature detection in the indirectly detected dimensions was obtained by the TPPI-States method.³⁶ 1D spectra were collected either with the normal sequence with water presaturation or using the WEFT sequence.³⁷ Spin-lattice relaxation times were measured using an inversion-recovery pulse sequence with a recycle time of $5T_1(^1H)$.

All data were processed using the FELIX program version 2.1 (Molecular Simulations Inc., San Diego, CA). The indirect dimensions of 2D data sets were multiplied by a skewed sine bell function and zero-filled to result in 1024×512 matrixes. For all 3D data sets, the number of data points in the indirect dimensions was increased by 25%

(29) Marion, D.; Driscoll, P.; Kay, L. E.; Wingfield, P.; Bax, A.; Gronenborn, A. M.; Clore, G. M. *Biochemistry* **1989**, *28*, 6150-6156.

(30) Kay, L. E.; Marion, D.; Bax, A. *J. Magn. Reson.* **1989**, *84*, 72-84.

(31) Ikura, M.; Bax, A.; Clore, G. M.; Gronenborn, A. M. *J. Am. Chem. Soc.* **1990**, *112*, 9020-9026.

(32) Bodenhausen, G.; Ruben, D. *Chem. Phys. Lett.* **1980**, *69*, 185-189.

(33) Bax, A.; Pochapsky, S. *J. Magn. Reson.* **1992**, *99*, 638-643.

(34) Sklenar, V.; Piotta, M.; Leppik, R.; Saudek, V. *J. Magn. Reson.* **1993**, *102*, 241-245.

(35) Shaka, A.; Keeler, J.; Frenkiel, T.; Freeman, R. *J. Magn. Reson.* **1983**, *52*, 335-338.

(36) Marion, D.; Ikura, M.; Tschudin, R.; Bax, A. *J. Magn. Reson.* **1989**, *85*, 393-399.

(37) Hochmann, J.; Kellerhals, H. *J. Magn. Reson.* **1980**, *38*, 23-39.

(26) Kurland, R.; McGarvey, G. *J. Magn. Reson.* **1970**, *2*, 286-301.

(27) Rajarathnam, K.; La Mar, G. N.; Chiu, M.; Sligar, S.; Singh, J.; Smith, K. *J. Am. Chem. Soc.* **1991**, *113*, 7886-7892. Kao, Y.-H.; Lecomte, J. T. *J. Am. Chem. Soc.* **1993**, *115*, 9754-9762.

(28) Tsan, P.; Caffrey, M.; Lawson, M.; Cusanovich, M. A.; Marion, D.; Gans, P., manuscript in preparation.

using linear prediction.³⁸ The resulting data were multiplied by a skewed sine bell function and zero-filled prior to Fourier transformation. Final 3D matrixes were $512 \times 128 \times 256$, $512 \times 128 \times 256$, and $512 \times 128 \times 128$ real points for the TOCSY–HSQC, NOESY–HSQC, and HSQC–NOESY–HSQC, respectively. For convenient analysis of 3D data sets, 2D strips were generated as previously described.³⁹

Computer Modeling. Calculation of a solution structure of *Rb. capsulatus* ferriCytc' has been hampered by the inability to assign backbone resonances in close proximity to the Fe center and the absence of observable NOEs between the heme moiety and the protein, due to paramagnetic effects on relaxation.^{10g} The geometric factors r , θ , and ϕ were therefore determined using the X-ray crystal structure of *Rb. capsulatus* ferriCytc'.⁴ For this analysis, the program InsightII (Molecular Simulations, Inc.) was used to add proton coordinates. The reference frame was defined as having the origin at the Fe, the Z-axis perpendicular to the plane defined by the pyrrolic nitrogens, the X-axis nearly lying along the N(III)–N(I) direction, and the Y-axis along the N(IV)–N(II) direction. All the calculations were made for the two crystallographic subunits of the dimer in order to account for possible atom position differences between them. The magnetic susceptibility tensor orientation was defined by the three Euler angles α , β , and γ relative to the molecular reference axes described above. The two anisotropic components of the magnetic susceptibility tensor were obtained from eq 2 by minimization of the following target function:

$$F = \sum_{\text{residue}} (\Delta\delta_{\text{obs}} - \delta_{\text{pm}})^2 \quad (5)$$

where $\Delta\delta_{\text{obs}}$ is the difference between the reduced and diamagnetic chemical shifts and δ_{pm} is calculated from eq 2. The residuals for the overall fits were defined as F/N where N is the number of residues. The residuals for the individual fits were defined as

$$\Delta\Delta\delta = \Delta\delta_{\text{obs}} - \delta_{\text{pm}} \quad (6)$$

The optimization of the three Euler angles α , β , and γ and the two components $\Delta\chi_{\text{ax}} = (\chi_{zz} - 1/2(\chi_{xx} + \chi_{yy}))$ and $\Delta\chi_{\text{rh}} = (\chi_{xx} - \chi_{yy})$ was achieved by means of a simulated-annealing algorithm developed in the laboratory.⁴⁰ As the axes x , y , and z are arbitrary; this gives up to six pairs of values of $\Delta\chi_{\text{ax}}$ and $\Delta\chi_{\text{rh}}$ related to one another by circular permutation of the x -, y - and z -axes and consequently to six degenerate minima with the same F/N . In agreement with the EPR convention of Blumberg,⁴¹ we chose the axis system in which the largest component is along z and the smallest along x (i.e., $|\chi_{zz}| > |\chi_{yy}| > |\chi_{xx}|$).

Structural changes were detected from the analysis of the residuals $\Delta\Delta\delta$ for each nucleus, as described by Feng et al.²³ Such changes are considered only if the difference between experimental and calculated dipolar shifts $|\Delta\Delta\delta|$ is larger than the estimated precision which arises both from the measurement of the chemical shifts (0.04 ppm for protons, 0.4 ppm for ¹⁵N) and the accuracy of the crystallographic coordinates Δl . The uncertainty associated with δ_{pm} depends on Δl and the atom position and can be evaluated by eq 7, which corresponds to the maximal variation of δ_{pm} for an atomic displacement of Δl . In the present study, Δl was taken as 0.3 Å for all the nuclei.

$$\Delta\delta_{\text{pm}} = \left(\left| \frac{\partial\delta_{\text{pm}}}{\partial r} \right| + \left| \left(\frac{1}{r} \right) \frac{\partial\delta_{\text{pm}}}{\partial\theta} \right| + \left| \left(\frac{1}{r \sin\theta} \right) \frac{\partial\delta_{\text{pm}}}{\partial\phi} \right| \right) \Delta l \quad (7)$$

EPR Spectra. EPR spectra were recorded with an X-band Bruker EMX spectrometer equipped with a dual-mode ER4116 cavity and an Oxford Instrument ESR-900 continuous-flow helium cryostat. The solution of 5 mM Cytc' was transferred to an EPR quartz tube. The tube was frozen, and the EPR spectra were recorded at 4 K in the parallel mode.

(38) Olejniczak, E.; Eaton, H. *J. Magn. Reson.* **1990**, *87*, 628–632.

(39) Caffrey, M.; Brutscher, B.; Simorre, J.-P.; Fitch, J.; Cusanovich, M.; Marion, D. *Eur. J. Biochem.* **1994**, *221*, 63–75.

(40) Blackledge, M.; Cordier, F.; Dosset, P.; Marion, D. *J. Am. Chem. Soc.* **1998**, *120*, 4538–4539.

(41) Gaffney, B. J.; Silverstone, H. J. In *EMR of paramagnetic molecules*; Berliner, L. J., Reuben, J., Eds.; Plenum Press: New York, 1993; Vol. 13, pp 1–57.

Magnetic Susceptibility Measurements. Data were collected on a 100- μL sample of ferriCytc', 3 mM heme concentration in D₂O, with an SHE model 905 SQUID susceptometer. Before measurements, the quartz sample holder was first left overnight in a HF solution to eliminate ferromagnetic contaminants, washed in distilled water, sonicated, and rinsed with distilled water. Measurements were made between 4.2 K and room temperature for three magnetic fields, 1, 2.5, and 5 T. The data were first corrected for the empty holder contribution, recorded under the same conditions. The diamagnetic contribution χ_{dia} from the protein and D₂O to the susceptibility was evaluated assuming that the susceptibility follows a polynomial law at high temperatures:

$$\chi_{\text{obs}}(T, H) \approx M_{\text{obs}}(T, H)/H = a_{\text{H}} + b_{\text{H}}T^{-1} + c_{\text{H}}T^{-2} \quad (8)$$

where a_{H} is an estimate of χ_{dia} . This value was then subtracted from the experimental data.⁴² Fits of the data were made assuming that the system is made of n moles of noninteracting heme units whose states are described by the classical effective spin Hamiltonian,⁴³

$$\mathcal{H} = \beta\mathbf{Sg}H + D[(S_z^2 - 1/3S(S+1))] + E(S_x^2 - S_y^2) \quad (9)$$

D and E are the ZFS axial and rhombic factors, respectively, and the \mathbf{g} -tensor is taken to be isotropic.

Data were adjusted by minimization of the residual

$$R = \sum_i \left(M_{\text{obs}}(T_i, H_i) - M_{\text{calc}}(T_i, H_i) \right) \frac{T_i}{H_i} \quad (10)$$

using the nearest-neighbor pivot method.⁴⁴ The calculated magnetization value $M(T_i, H_i)$ is given by the formula

$$M(T_i, H_i) = nN_{\text{A}}k_{\text{B}}T_i \int \sin\theta \, d\theta \int \frac{d\varphi}{4\pi} \left[\frac{\partial(\ln Z(T_{-i}, H, \theta, \varphi))}{\partial H} \right]_{H=H_i} \quad (11)$$

where N_{A} is the Avogadro number and $Z(T_{-i}, H, \theta, \varphi)$ the system partition function for an orientation θ , φ in the magnetic field system's frame.⁴³

Results

Magnetic Susceptibility and Electron Paramagnetic Resonance Spectroscopy Results. To characterize the spin state of the iron(II) in the *Rb. capsulatus* ferriCytc', we performed magnetic susceptibility measurements and EPR spectroscopy. Figure 1 illustrates the temperature dependence of the molar effective magnetic moment observed in the ferriCytc' sample for three applied magnetic fields. The values taken by the molar effective magnetic moment above 100 K are in the range 4.8–5.2 μ_{B} and are, therefore, in good agreement with the value expected for 1 mol of isolated spin quintuplet: 4.90 μ_{B} .⁴³ No excited state having a spin value different from that of the ground state is thermally accessible, at least below 1000 K, as indicated by the absence of a wide variation of the effective magnetic moment between 100 and 250 K.

In Figure 2, the molar magnetization is plotted against the field/temperature ratio for the three magnetic fields. The difference observed between the three isofield curves indicates the presence of a strong ZFS interaction.⁴² The solid lines shown in Figures 1 and 2 correspond to the adjustment results. The adjustment has been performed using the assumptions described in the Materials and Methods section and the results are shown in Table 1. The derived ZFS interaction parameters are –18.3

(42) Day, E. P.; Kent, T. A.; Lindhal, P. A.; Münck, E.; Orme-Johnson, W. H.; Roder, H.; Roy, A. *Biophys. J.* **1987**, *52*, 837–853.

(43) Kahn, O. *Molecular Magnetism*; VCH Publishers: New York, 1993.

(44) Serra, P.; Stanton, A. F.; Kais, S. *J. Chem. Phys.* **1997**, *106*, 7170–7177.

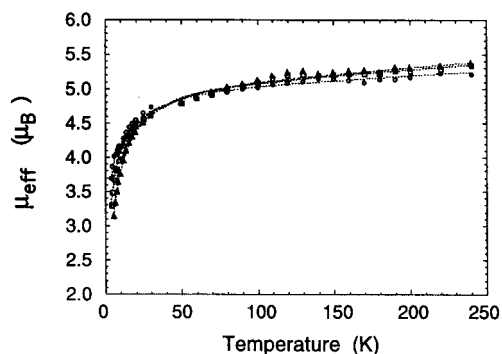


Figure 1. Temperature dependence of the molar effective magnetic moment of the ferrocyclochromes *c'* from *Rb. capsulatus* for three values of the applied magnetic field. Circle = 1 T, square = 2.5 T, triangle = 5 T. The three lines through the data are the magnetic moment curves calculated using the effective spin Hamiltonian ($g = 2$, $D = -18.3 \text{ cm}^{-1}$, and $E/D = 0.27$). The molar effective magnetic moments in the range 4.8–5.2 μ_B are in good agreement with the value 4.90 μ_B expected for an isolated $S = 2$ spin-state.

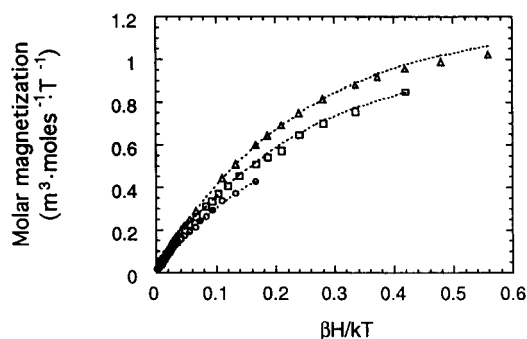


Figure 2. Molar magnetization of the ferrocyclochromes *c'* of *Rb. capsulatus* plotted against $\beta H/kT$ for three values of the applied magnetic field. Circle = 1 T, square = 2.5 T, triangle = 5 T. The three lines through the data are magnetization curves calculated using the effective spin Hamiltonian ($g = 2$, $D = -18.3 \text{ cm}^{-1}$, and $E/D = 0.27$). The presence of a strong ZFS interaction is indicated by the nonsuperposition of the isofield curves.

Table 1. Calculated Zero-Field Splitting and Rhombic Splitting Factor

H (T)	n^a	D (cm^{-1})	η^b	TIC ^c	residual ^d
1	0.303	-16.4	0.28	4.74	4.5
2.5	0.305	-19.5	0.30	6.60	5.7
5	0.306	-19.5	0.28	7.25	5.4
simult ^e	0.304	-18.3	0.27	<i>f</i>	18.8 ^g

^a Number of micromoles of paramagnetic iron center in the sample. This value was fitted during the calculation. ^b E/D ratio. ^c Temperature-independent correction: deals with the uncertainty present in the estimate of χ_{dia} with eq 8 (in 10^{-10} emu). ^d Residual of the fit. Values are given in $10^{-15} \text{ emu}^2 \cdot \text{K}^2$. ^e A unique set of data was used for the simultaneous fit of the three isofield curves. ^f TIC values for the isofield curves at 1, 2.5, and 5 T are 5.00, 6.74, and 7.34, respectively. ^g Sum of the residuals for the three isofield curves.

cm^{-1} for the D factor and 0.27 for the rhombic factor E/D . A slight disagreement between the data and the fit has been observed only at very low temperatures for the strong magnetic field value of 5 T and could be due to intermolecular antiferromagnetic coupling.

The EPR spectrum of a frozen solution of ferroCyt c' has been recorded using the parallel mode (Figure S1, Supporting Information). A single large asymmetric resonance signal is observed with a minimum at $g = 8.38$. This spectrum displays a similar shape and frequency as for other high-spin ferro

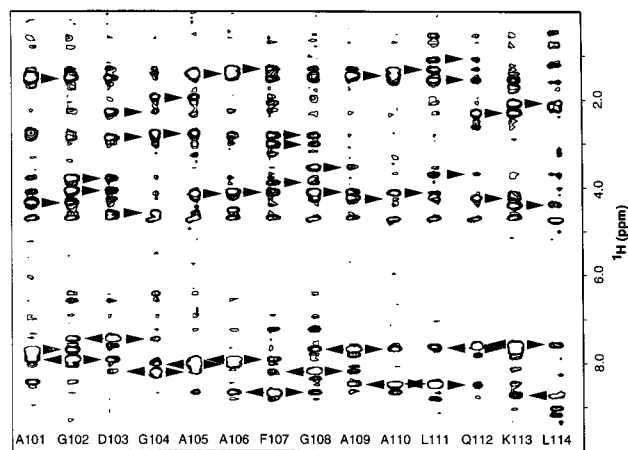


Figure 3. 2D representation of the NOESY-HSQC 3D experiment for the sequential assignment of *Rb. capsulatus* ferrocyclochromes *c'* residues A101-L114. The mixing time was 120 ms. Each residue is presented as a small region of the 2D spectrum taken at the ^{15}N frequency and centered at the $^1\text{H}^{\text{N}}$ frequency (Table S1, Supporting Information). Arrows are drawn for short-range interresidue NOEs. The presence along the sequence of consecutive d_{NN} is characteristic of a helical conformation between A101 and L114.

compounds, such as deoxymyoglobin or model compounds,⁴⁵ and therefore is in agreement with the proposed spin state of the iron in the ferroCyt c' .

Cytochrome *c'* Assignment. (a) Spin System Identification. In the TOCSY-HSQC 3D experiment, intraresidue $\text{H}^{\text{N}}-\text{H}^{\alpha}$ correlations are observed for 106 of 126 non-proline amino acids, and $\text{H}^{\text{N}}-\text{H}^{\beta}$ correlations are observed for 86 of 112 non-proline and non-glycine amino acids. In contrast, correlations for the H^{γ} , H^{δ} , etc. are missing for many long-chain amino acids. The missing $\text{H}^{\text{N}}-\text{H}^{\alpha}$ correlations in the TOCSY-HSQC experiment are presumably due to increased transverse relaxation rates of the H^{N} , H^{α} , or ^{15}N nuclei close to the paramagnetic center. In addition to this effect, the incomplete TOCSY transfer in the long side chain could originate from the slow tumbling rate of the protein. Finally, we note that a single set of resonances is present in the TOCSY-HSQC experiment for the reduced state, indicating that the ferroCyt c' complex either is in a monomeric state or is a symmetric dimer, as previously observed for the ferriCyt c' by X-ray crystallography.^{4a,b}

(b) Sequential Assignment and Secondary Structure. The ^1H and ^{15}N resonances of *Rb. capsulatus* ferroCyt c' were sequentially assigned by the NOESY-HSQC 3D experiment, in which $^1\text{H}^{\text{N}}-^{15}\text{N}$ pairs are correlated to intra- and interresidue ^1H ,²⁹ and by the HSQC-NOESY-HSQC 3D experiment, in which $^1\text{H}^{\text{N}}-^{15}\text{N}$ pairs are correlated to interresidue ^{15}N .³¹ Assignment of residues A101 to L114 using NOESY-HSQC is illustrated in Figure 3. In this figure, each residue is represented by a small region of the 2D plane at a given ^{15}N frequency and centered at a given $^1\text{H}^{\text{N}}$ frequency. Short-range $d_{\text{N}(i,i+1)}^{\text{N}}$, $d_{\text{N}(i,i+1)}^{\text{N}}$, and $d_{\text{N}(i,i+1)}^{\beta}$ connectivities are shown by horizontal lines. A summary of the short-range and medium-range ($d_{\text{N}(i,i+3)}^{\text{N}}$) connectivities observed in NOESY-HSQC is given in Figure 4. In addition, the relative H^{N} exchange rates are presented. Together the $d_{\text{N}(i,i+3)}^{\text{N}}$ connectivities and HN exchange rates suggest that there are four helical regions in *Rb. capsulatus* ferroCyt c' : residues 3–29, 33–49, 78–97, and 103–117. In total, backbone ^1H and ^{15}N have been assigned for 116 of the 126 residues present in *Rb. capsulatus* Cyt c' .

(45) Hendrich, M. P.; Debrunner, P. G. *Biophys. J.* **1989**, *56*, 489–506. Yu, B.-S.; Goff, H. M. *J. Am. Chem. Soc.* **1989**, *111*, 6558–6562.

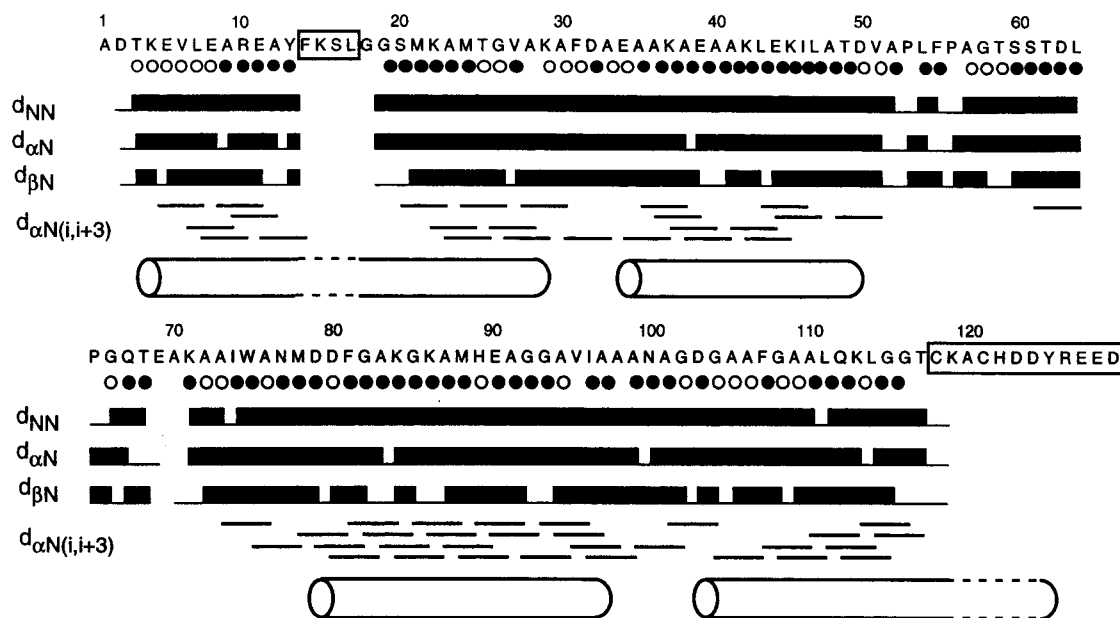


Figure 4. Schematic summary of the sequential connectivities for the assignment of *Rb. capsulatus* ferrocytochrome *c'*. No distinctions are made for the relative intensities of the NOEs because the presence of the centrally located paramagnetic center leads to nonuniform relaxation rates within the molecule. Unassigned residues are boxed. H^N in slow exchange ($t_{1/2} > 5$ min) are identified by filled circles, and H^N in fast exchange ($t_{1/2} < 5$ min) are identified by open circles. The helical regions identified by the $d_{\alpha N(i,i+3)}$ and slowly exchanging H^N are shown by solid lines. The dotted lines for helix-1 and helix-4 represent the expected helical structure based on the X-ray structure of *Rb. capsulatus* ferriCyt*c'*.⁴

(c) Assignment of Side-Chain ^{15}NH . The side-chain ^{15}NH resonances of Q67, W75, N77, N100, and Q112 were identified by the TOCSY–HSQC 3D experiment and assigned by the NOESY–HSQC 3D experiment. Specifically, the side-chain ^{15}NH of W75 was assigned by a TOCSY correlation to the C_2H , which exhibits NOEs to the previously assigned H^α and H^β of W75. The side-chain ^{15}NH s of N77 and N100, and of Q67 and Q112, were assigned by NOEs between the ^{15}NH and the previously assigned H^α and H^β , H^β and H^γ , respectively. In contrast, the side-chain ^{15}NH s of R10, H89, H122, and R126 were not apparent in the TOCSY–HSQC or NOESY–HSQC 3D experiments. A summary of the chemical shifts is given in the Supporting Information.

(d) Assignment of the Iron(II) Ligand Protons. In Figure 5, a 1D spectrum of the ferroCyt*c'* of *Rb. capsulatus* is shown. This spectrum is similar to those reported for the ferroCyt*c'* of *Chromatium vinosum*, *Rhodospirillum rubrum*, and *Rhodocyclus gelatinosus*,^{10a,e–f} with the classical pattern of three methyl resonances shifted upfield and the fourth downfield. We observe several large resonances shifted out of the “diamagnetic” envelope and whose chemical shifts, T_1 relaxation times, and proposed assignments are reported in Table 2, together with those of homologous Cyt*c'*. Heme protons have been assigned using 2D NOESY experiments in 2H_2O and 1D NOE experiments. First, the assignment has been initiated at the four CH_3 resonances at -5.5 , -9.14 , -12.1 , and 16.5 ppm. The NOE observed between the resonance at -12.1 and -5.5 ppm supports the assignment of adjacent methyl-2 and methyl-18 (data not shown). Propionate-17 α -protons were identified as resonance pairs correlated by strong NOE with one of these two methyls, therefore assigned to methyl-18. Propionate-13 α -protons were identified as resonance pairs correlated by strong NOE with one of the two remaining methyls, which was consequently assigned as methyl-12. Methyl-3 and methyl-8 have been tentatively assigned as giving the strongest correlations with methyl-2 and methyl-7, respectively. The β -protons and N_1H of His122 were assigned following the assignments of similar signals in homologous Cyt*c'* or deoxymyoglobins.^{10a,f}

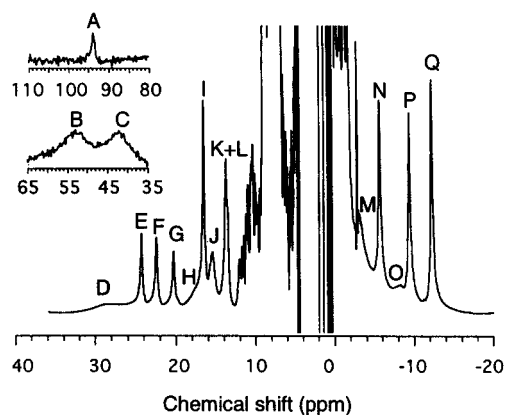


Figure 5. 1D spectra of the ferrocytochrome *c'* of *Rb. capsulatus*. This spectrum shows the general but unusual pattern of three upfield and one downfield methyl resonances of ferroCyt*c'*. The full spectrum was recorded with a water presaturation of 150 ms, a spectral width of 25 000 Hz, and 200 000 scans. Insets were taken from a spectrum recorded at 315 K using a WEFT sequence³⁷ with a spectral width of 100 000 Hz, 1024 scans, a recycling time of 10 ms, and a relaxation time of 30 ms between the 90° pulses and the refocalizing pulse. A, His122 N_1H ; B, His122 C_4H ; C, His122 C_2H ; E, propionate 17 1 ; F, His122 β ; G, propionate 13 1 ; I, methyl-7 1 ; K, His122 β' ; L, propionate 13 1 ; N, methyl-2 1 ; P, methyl-12 1 ; Q, methyl-18 1 . Tentative assignments for peaks D, H, J, and M are reported in Table 5. I, N, P, and Q peaks integrate for three protons; J, K, and L peaks integrate for more than one proton.

The α -proton of His122 was assigned as giving the strongest NOE correlations with the β -protons. We assigned tentatively the resonances at 47 and 55 ppm ($\Delta\nu = 3000$ Hz) to the C_2H and C_4H of the imidazole of His122 on the basis of similar features in the deoxymyoglobin and model compounds.^{17a} As indicated in Table 2, these assignments are in agreement with those reported for the *R. gelatinosus* Cyt*c'*.^{10f}

Magnetic Susceptibility Tensor Determination. Magnetic properties of the reduced state as well as potential structural differences between states can be assessed using eq 2. It is,

Table 2. Chemical Shift and Longitudinal Relaxation Time of the Ligand Protons in *Rb. capsulatus* Ferrocyclochrom *c'* and Relative Compounds

proton ^b	chemical shift (ppm) ^a			
	caps ^c	gelat ^d	vinos ^e	rub ^f
methyl-2 ¹ (N)	-5.49 (43)	-9 (35)	-7.5	-8
thiomethyl-3 ²	0.5			
thiomethine-3 ¹				
methyl-7 ¹ (I)	16.53 (38)	17 (45.1)	18.5	23
thiomethyl-8 ²	-1.5			
thiomethine-8 ¹				
methyl-12 ¹ (P)	-9.14 (42)	-12 (36.4)	-12.2	-10
propionate-13 ¹ (G)	20.4 (45)	20.5 (56)		
propionate-13 ¹ (L)	13.77 (24)	14 (34)		
propionate-17 ¹	12.19 (17)	11		
propionate-17 ¹ (E)	24.18 (41)	24 (17.2)		
methyl-18 ¹ (Q)	-12.1 (43)	-14 (38.2)	-16.6	-12
His β (β') (K)	13.8 (30)	14 (22.3)		
His β' (β) (F)	22.6 (23)	24 (13.2)		
His N1H (A)	100.6		104	
His C ₂ H (C)	47 (<1)			
His C ₄ H (B)	55 (<1)			

^a Chemical shifts are referenced to the H₂O resonance and are accurate to ± 0.02 ppm. ^b Heme protons are named following the IUPAC recommendations. Letters in parentheses correspond to the peak labeling in Figure 5. ^c This work, measured at 300 K, pH 6.0. In parentheses are indicated the T_1 in milliseconds. The T_1 values were obtained by fitting the peak intensities as a function of the delay in inversion-recovery measurements. ^d Heme protons chemical shifts and longitudinal relaxation times of the ferroCyt c' from *R. gelatinosus* recorded at 295 K and pH 5.0.^{10f} ^e Proton chemical shifts of the ferroCyt c' from *C. vinosum* recorded at 298 K and pH 7.2.^{10e} Assignments of the methyl protons are only tentative and based on chemical shift values. ^f Proton chemical shifts of the ferroCyt c' from *Rsp. rubrum* recorded at 303 K.^{10a} Assignments are only tentative and based on chemical shift values.

however, necessary to assume that the electron density of the ferrous state is located at the Fe center, a simplification which is only justified for nuclei that are located at least 10 Å away from the metal center.⁴⁶ This criterion is satisfied by all of the backbone nuclei considered in the present discussion.

The magnetic susceptibility tensor components can be derived from eq 2 by a least-squares fitting. H^N chemical shifts were initially excluded from the calculation because they are sensitive not only to paramagnetic effect but also to H-bonding.⁴⁷ ¹⁵N chemical shifts were also excluded from the initial calculation because they are sensitive to interactions between the ¹⁵N atomic orbitals and those of neighboring atoms,⁴⁸ in addition to H-bonding and paramagnetic effects. Glycine H^a shifts were excluded, as they were not stereospecifically assigned. In the initial stage, we used the complete set for 89 H^a and the coordinates of the A subunit. The fit resulted in $\Delta\chi_{ax} = 3.82 \times 10^{-33}$ m³ and $\Delta\chi_{rh} = -1.12 \times 10^{-33}$ m³, with F/N = 4.1×10^{-3} ppm² (Table 3). Surprisingly, the z-axis of the χ -tensor was found to be tilted approximately 30° away from the heme normal axis. The whole conformational space was thus explored in order to look for other minima on the heme symmetry axes. We found no minima other than the six expected by circular permutation of the x-, y- and z-axes (see Materials and Methods). Therefore, for the following calculation stages, the conformational space exploration was restricted to the quadrant containing the minimum corresponding to $|\chi_{zz}| > |\chi_{yy}| > |\chi_{xx}|$. A com-

(46) Golding, R.; Pascual, R.; Stubbs, L. *Mol. Phys.* **1976**, *31*, 1933.

(47) Wagner, G.; Pardi, A.; Wuthrich, K. *J. Am. Chem. Soc.* **1983**, *105*, 5948–5949.

(48) Martin, G.; Martin, M.; Gouesnard, J. *¹⁵N NMR Spectroscopy*; Springer: New York, 1981. Glushka, J.; Lee, M.; Coffin, S.; Cowburn, D. *J. Am. Chem. Soc.* **1989**, *111*, 7716–7722. Braun, D.; Wider, G.; Wuthrich, K. *J. Am. Chem. Soc.* **1994**, *116*, 8466–8469.

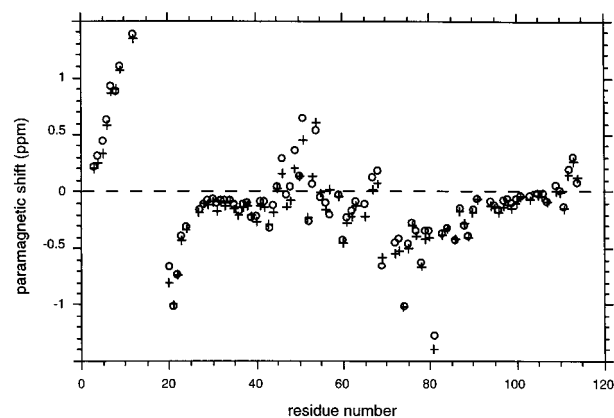


Figure 6. Comparison of the observed and calculated H^a paramagnetic chemical shifts for the ferrocyclochrom *c'* of *Rb. capsulatus*. Open circles: calculated paramagnetic chemical shifts; crosses, observed paramagnetic chemical shifts. The H^a shifts of glycines were excluded, due to the absence of stereospecific assignments. Values are $\alpha = 39^\circ$, $\beta = 26^\circ$, $\gamma = 6^\circ$, $\Delta\chi_{ax} = 3.82 \times 10^{-33}$ m³, $\Delta\chi_{rh} = -1.15 \times 10^{-33}$ m³.

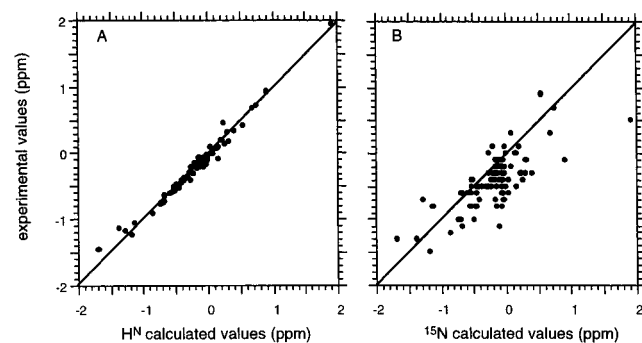


Figure 7. Comparison of the experimental paramagnetic chemical shifts of the H^N (A) and ¹⁵N (B) with the calculated dipolar shifts calculated with the results obtained from the H^a set. Values are $\alpha = 39^\circ$, $\beta = 26^\circ$, $\gamma = 6^\circ$, $\Delta\chi_{ax} = 3.82 \times 10^{-33}$ m³, $\Delta\chi_{rh} = -1.15 \times 10^{-33}$ m³. The line corresponds to the $y = x$ function.

parison of the observed and calculated H^a chemical shifts (Figure 6) illustrates the very good agreement between the data and the calculation. On the second unit of the dimer, similar results were obtained for the orientation and the amplitudes of the χ -tensor components (Table 3). The H^N and ¹⁵N dipolar shifts calculated from the optimized parameters obtained with the H^a set are shown in Figure 7 as a function of the experimental values for the A subunit. As illustrated by this figure, the calculated paramagnetic shifts for H^N fit very well with the experimental shifts. Calculations with the H^N or ¹⁵N chemical shifts performed for the two subunits are reported in Table 3. We found the same orientation and the same axial susceptibility anisotropy for all sets of protons. Only a slight variation of less than 15% is observed for the rhombic anisotropy. The ¹⁵N set also gives comparable values of the axial and rhombic anisotropy but yields a slightly lower tilt of the z-axis.

In a second stage, atoms which exhibited $|\Delta\Delta\delta|$ larger than the sum of the experimental error of the chemical shift (0.04 ppm for ¹H and 0.4 ppm for ¹⁵N) and the uncertainty due to the accuracy of the coordinates (see Materials and Methods) (i.e., 13 H^a, 13 H^N, and 20 ¹⁵N of subunit A and 10 H^a, 12 H^N, and 19 ¹⁵N of subunit B) were discarded from the calculation.⁴⁹ The fit for the proton sets resulted in the same values of the orientation as well as the amplitude of the axial and rhombic anisotropy (Table 3). In contrast, using the restricted ¹⁵N set gave a comparable tilt of the z-axis but larger values of the axial and rhombic anisotropy.

Table 3. Calculated Angles and Components of the Magnetic Susceptibility Tensor for the Ferrocycytochrome *c'* of *Rb. capsulatus*

atom set (subunit)	α^a (deg)	β^a (deg)	γ^a (deg)	$\Delta\chi_{ax}^b$	$\Delta\chi_{rh}^b$	F/N^c
Full Set						
89 H $^\alpha$ (A)	40	27	3	3.82	-1.12	4.1
89 H $^\alpha$ (B)	42	28	1	3.86	-1.13	3.9
101 H N (A)	37	27	9	3.89	-0.91	4.0
101 H N (B)	38	28	8	3.95	-0.92	3.6
101 ^{15}N (A)	24	25	23	3.44	-1.19	129.4
101 ^{15}N (B)	26	22	17	3.27	-1.15	141.3
89 H $^\alpha$ + 101 H N (A)	37	27	7	3.84	-1.00	4.2
89 H $^\alpha$ + 101 H N (B)	39	28	6	3.90	-1.00	4.0
Restricted Set						
76 H $^\alpha$ (A)	39	26	6	3.82	-1.15	2.3
79 H $^\alpha$ (B)	41	27	3	3.85	-1.16	2.3
88 H N (A)	35	28	11	3.85	-0.87	3.0
89 H N (B)	38	28	8	3.89	-0.86	3.2
81 ^{15}N (A)	20	26	30	4.51	-1.46	45.5
82 ^{15}N (B)	20	28	33	4.72	-1.67	43.0
76 H $^\alpha$ + 91 H N (A) ^d	36 (0.5)	27 (0.3)	9 (1)	3.84 (0.05)	-1.01 (0.09)	3.1
79 H $^\alpha$ + 90 H N (B)	39	28	6	3.89	-1.01	3.1

^a The component axes were chosen following the Blumberg convention.⁴¹ ^b In 10^{-33} m³. ^c In 10^{-3} ppm². ^d The numbers in parentheses correspond to the uncertainties calculated using Monte Carlo simulations.⁵⁰

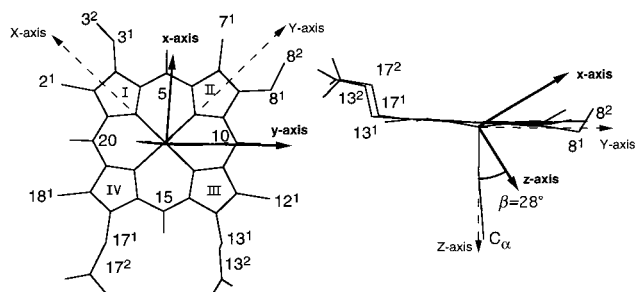


Figure 8. Position of the magnetic susceptibility tensor in the ferrocycytochrome *c'* of *Rb. capsulatus*. On the right-hand side, the heme has been rotated 90° around the heme normal with respect to the left side. Location of the imidazole ligand is the inverse in the Cyt c' with respect to myoglobins. Heme substituents were named following the IUPAC recommendations. The molecular axes (*X*, *Y*, *Z*) have the *Z*-axis normal to the heme, with the *X*-axis oriented following the N(III)–N(I) direction, and are in dashed lines. The magnetic axes (*x*, *y*, *z*) are indicated in bold lines, with the *y*-axis pointing toward the front of the figure.

In a last stage, the procedure has been repeated with the combined sets of H $^\alpha$ and H N chemical shifts, and these final values are discussed. Uncertainties on the orientation and the principal component values have been estimated using Monte Carlo simulations⁵⁰ and are reported in Table 3. The principal axes of the χ -tensor are shown in Figure 8. From the values of $\Delta\chi_{ax}$ and $\Delta\chi_{rh}$, we have calculated a ZFS axial parameter *D* of -23.8 ± 0.2 cm⁻¹ and a ZFS rhombic factor *E* of -3 ± 0.1 cm⁻¹ from eqs 3 and 4, assuming that the system can be described by eq 9 with an isotropic **g**-tensor.

Last, calculations assuming a dimeric state for the Cyt c' were performed but no improvement of the fit was obtained.

Contact Shift of the Iron Ligands. In accordance with the metal-centered hypothesis, the magnetic susceptibility tensor was determined using protons located 10 Å and more away from the iron center. For other protons, a rigorous calculation of the

(49) The following atoms were excluded from the fit. H $^\alpha$: 5, 20, 31, 48, 49, 57, 65, 67, 72, 73, 97, 98, and 99 in subunit A; 20, 31, 48, 49, 57, 65, 73, 79, 97, 98, and 99 in subunit B. H N : 23, 25, 26, 27, 31, 33, 39, 41, 54, 74, 77, 79, and 81 in subunit A; 23, 25, 26, 27, 31, 33, 39, 41, 43, 74, and 79 in subunit B. ^{15}N : 4, 5, 6, 7, 9, 12, 22, 32, 34, 39, 47, 49, 59, 68, 72, 74, 86, 104, and 108 in subunit A; 4, 5, 6, 9, 12, 32, 34, 39, 42, 47, 49, 51, 59, 68, 72, 74, 77, 86, 104, and 108 in subunit B.

(50) Cordier, F.; Caffrey, M.; Brutscher, B.; Cusanovich, M. A.; Marion, D.; Blackledge, M. *J. Mol. Biol.* **1998**, *281*, 341–361.

Table 4. Dipolar and Contact Contribution in the Paramagnetic Chemical Shifts of the Heme Protons of *Rb. capsulatus* Ferrocycytochrome *c'* and Sperm Whale Deoxymyoglobin

heme atom ^d	chemical shift (ppm)				
	param ^b	dipolar ^c	contact ^d	SWM dip ^e	SWM cont ^e
methyl-2	-9.2	-7.4	-1.8	-3.12	7.2
thiomethyl-3	-1.8	-3.05	1.3		
thiomethyne-3			-2.4		
methyl-7	12.7	-2.8	15.5	2.17	4.9
thiomethyl-8	-3.1	-3.4	0.3		
thiomethyne-8		-8.2			
methyl-12	-12.9	-7.1	-5.8	-2.36	15.7
propionate-13 ^{1f}	16	-2.3	18	-1.64	7.9
propionate-13 ^{1f}	10	-3.0	13	-0.70	1.7
propionate-17 ^{1f}	20	-0.3	20	2.09	6.9
propionate-17 ^{1f}	9	-2.4	11	2.65	4.11
methyl-18	-15.7	-6.0	-9.7	0.62	3.5
5-H		-3.3			
10-H		-19.2			
15-H		1.9			
20-H		-19.9			

^a Nomenclature of the heme protons of the ferroCyt c' followed IUPAC recommendations. ^b Obtained from the difference between ferroCyt c' and the diamagnetic CO complex.²⁸ ^c Calculated from the values of magnetic susceptibility tensor determined in this work and the coordinates of the heme protons of the ferriCyt c' structure.^{4b} ^d Obtained from the difference of the observed paramagnetic shift and the calculated values of the dipolar shift. ^e From ref 16. ^f Paramagnetic shifts of the propionate protons have been estimated using values measured in the reduced cytochrome *c*₅₅₁ of *Ectothiorhodospira halophila*,⁶² as they have not been specifically assigned in the diamagnetic form.

dipolar shift should include a ligand-centered contribution.⁵¹ However, this approach still provides an estimate for the dipolar shift, which has been used to derive the contact shift for the ligand protons. The calculated dipolar and contact shifts are compared with the data on sperm whale deoxymyoglobin¹⁶ in Table 4. We observe positive contact shifts and consequently high positive spin density delocalization on C7¹, C13¹, and C17¹ for the *Rb. capsulatus* ferroCyt c' . In contrast, C2¹, C12¹, and C18¹ experience weak and negative contact shifts. Contact contribution of 1.2 ppm is observed for thiomethyl-3, which suggests the presence of a significant spin delocalization on C3¹.

(51) Bertini, I.; Luchinat, C. In *NMR of paramagnetic molecules in biological systems*; Lever, A. B. P., Gray, H. B., Eds.; The Benjamin/Cummings Publishing Co.: Menlo Park, NJ, 1986; pp 47–84.

Table 5. Predicted Values of the Chemical Shift and the Longitudinal Relaxation Times for the Protons of the Heme Cavity in the Ferrocycytochrome *c'* of *Rb. capsulatus*

residue	atom	$D_{\text{Fe-H}}^a$ (Å)	T_1^b (ms)	δ_{dip}^c (ppm)	δ_{calc}^d (ppm)	δ_{err}^e (ppm)	peak ^g
F14	HN	6.9	93	7.6	15.6	1.2	
F14	HA	5.09	15	10.7	15.5	3.7	
F14	HB1	3.97	3	23.5	25.3	9.8	D
F14	HB2	5.3	20	14.2	16.5	3.2	J
F14	HD ^{*f}	4.38	1.5	27.4	35.0	22.2	
F14	HE ^{*f}	4.58	2	5.1	12.5	7.9	
F14	HZ	4.77	12	0.7	8.3	2.5	
L17	HB1	6.16	47	-4.8	-4.1	1.2	
L17	HB2	5.6	27	-1.1	-0.6	1.1	
L17	HD1 ^{*f}	5.30	9	-1.9	-2.6	2.2	
G18	HN	6.82	87	-2.5	6.7	0.9	
F55	HZ	6.17	47	-0.4	6.3	1.0	
C118	HA	4.98	13	9.7	13.5	3.7	K or L
C118	HB1	4.68	9	9.8	12.2	4.5	
C118	HB2	6.39	60	5.2	6.4	1.4	
C121	HB1	5.13	16	0.6	2.7	0.4	
C121	HB2	6.69	76	3.1	5.1	2.3	
H122	HN	5.66	28	10.8	17.6	2.9	K or L
H122	HA	5.58	25	3.8	6.4	2.0	
R126	HB1	6.26	52	-0.6	2.0	0.8	
R126	HB2	5.24	17	-5.6	-3.2	1.8	M ^h
R126	HG1	6.16	47	-4.1		0.8	
R126	HG2	6.98	100	-1.9		0.5	
R126	HD1	5.16	16	-0.6		1.5	
R126	HD2	3.98	3	-9.6		4.8	

^a Distance between the iron center and the proton calculated from the coordinates of the oxidized form.^{4b} ^b Calculated from $T_{1\text{H}} = T_{1\text{Met}}(r_{\text{Fe-H}}/r_{\text{Fe-Met}})^6$, with $T_{1\text{Met}} = 40$ ms. ^c δ_{dip} was calculated using the orientation and the optimized magnetic tensor $\alpha = 36^\circ$, $\beta = 27^\circ$, $\gamma = 9^\circ$, $\Delta\chi_{\text{ax}} = 3.84 \times 10^{-33}$ m³, $\Delta\chi_{\text{rh}} = -1.01 \times 10^{-33}$ m³, and the coordinates of the oxidized form.^{4b} ^d Calculated as the sum of the chemical shifts measured in the diamagnetic form²⁸ and δ_{dip} . ^e Calculated from the uncertainty on the coordinates as described in Materials and Methods. ^f For protons of aromatic rings or methyl groups, we take as the relaxation time the estimation of the relaxation time for the nearest proton of the metal center and as the dipolar or chemical shift value the mean of the dipolar or chemical shift of the protons in chemical exchange. ^g Tentative assignment from the similarity between the measured parameters and calculated parameters. The letters correspond to the peak labeling in Figure 5. ^h The T_1 value of M peak is 20 ± 5 ms.

Assignments of Protons Located in the Heme Cavity. The electronic relaxation time in the ferroCyt c' can be derived from the heme methyl T_1 under the assumption of a purely dipolar relaxation with the electron.⁵¹ This assumption seems reasonable as the T_1 values for the four methyls groups are rather similar despite very different contact shifts (Tables 2 and 4). From the observed values of T_1 , we obtain an electronic relaxation time of about 4×10^{-9} s, of the same order of magnitude as those reported for deoxymyoglobin and deoxyhemoglobin.⁵¹

The ^1H T_1 in the heme cavity can then be predicted using the structure coordinates of the oxidized form and the relation

$$T_{1\text{H}} = T_{1\text{Met}} \left(\frac{r_{\text{Fe-H}}}{r_{\text{Fe-Met}}} \right)^6 \quad (12)$$

In the same way, the chemical shift of these protons can be estimated from their chemical shift in the diamagnetic CO complex form and the calculated dipolar shift. From the data predicted for these protons, resonances out of the "diamagnetic" part of the spectrum have been tentatively assigned and are reported in Table 5.

Discussion

In this study, we have characterized the reduced paramagnetic form of a Cyt c' . This allows us to gain some insights into the

structural and magnetic properties of the physiological form of a Cyt c' . We assigned for the first time the backbone nuclei of a ferrous high-spin hemoprotein. The remaining unassigned residues correspond to those in close proximity to the heme binding site (F14–L18, C118–E127) and hence the paramagnetic center.

Structural Properties of the Ferrocycytochrome *c'*. As no structure is yet available, very little information is available on the ferrocycytochrome *c'*, in particular in the direct neighborhood of the iron. Our results allows us to gain structural insights into this physiological form. First, the secondary structure of the reduced state consists of four helices, helix-1 (3–30), helix-2 (34–49), helix-3 (78–97), and helix-4 (103–117), and does not show significant differences from that of the oxidized state and the diamagnetic state, as derived by NMR spectroscopy^{10g,28} and X-ray crystallography.⁴ Dipolar shift analysis for the reduced state of *Rb. capsulatus* Cyt c' has allowed us to probe for redox-dependent structural changes. Generally, protons that exhibit chemical shifts in poor agreement with the calculated shift are interpreted as undergoing redox-dependent structural changes. Accordingly, considering the H^α data set, redox-dependent structural changes appear to be very limited between the reduced and the diamagnetic state as well as between solution and crystal states. Protons that show deviations above the criterion defined in Materials and Methods are primarily located in the loop regions. Moreover, the fair agreement for the amide protons supports the lack of major changes in the hydrogen bond networks involving these nuclei between the different redox forms. In contrast, the agreement between the observed and calculated paramagnetic shifts for the ^{15}N backbone atoms is quite poor, as is that in the oxidized form.²⁸ Such a situation has been also observed for the only other known example: cytochrome b_5 .^{24b} At this time, we have no explanation for this different behavior.

Redox-dependent change could be expected in the iron environment. Indeed, in the CO complex diamagnetic state, the hexacoordinated iron is thought to be in the porphyrinic plane as in the *N*-butylisocyanide complex,^{4a} whereas the iron is displaced out of the plane in the pentacoordinated high-spin state, as shown by model compounds or myoglobin structures.⁵² Moreover, the coordination of the carbon monoxide could lead to a displacement of some residues around the coordination site for ligand fitting. Unfortunately, due to the relaxation induced by the paramagnetic iron, the structural probes on the backbone are too scarce for a precise description of this region, and the paramagnetic shifts cannot be efficiently used because of line broadening. The agreement of the predicted chemical shifts and T_1 values of some of the protons located in the heme cavity with the chemical shifts and T_1 values of resonances observed outside of the diamagnetic part suggests, however, that iron reduction does not induce large structural changes in the heme environment. Assignment of these protons is underway to investigate more precisely this point.

Finally, most backbone nuclei do not exhibit anomalous chemical shifts and are thus not experiencing structural changes between the different redox states of *Rb. capsulatus* Cyt c' . This observation is in agreement with previous NMR studies on other heme proteins not related to the Cyt c' . For example, redox-dependent structural changes were limited to a few residues in the cytochromes c ,^{22,23} cytochrome b_5 ,²⁴ and myoglobin.²⁷ Together, these observations support the lack of large-scale structural changes in heme proteins.

(52) Scheidt, W., R.; Gouterman, M. In *Iron Porphyrin, Part I*; Lever, A. B. P., Gray, H. B., Eds.; Addison-Wesley Publishing Co.: Reading, MA, 1982; pp 89–139. Takano, T. *J. Mol. Biol.* **1977**, *110*, 569–584.

Magnetic Properties of the Ferrocyclochrome *c'*. Magnetic susceptibility measurements show that the iron(II) is in a thermally isolated spin state. Besides, no admixing of spin states take place in the reduced form, in contrast with the oxidized form. Although a spin state lower than 2 with a significant orbital contribution cannot be formally excluded, the value of the effective magnetic moment is that of a spin-only $S = 2$ state, which is in agreement with the spin state expected from the pentacoordination of the iron. Assuming that the system can be described by eq 9 with an isotropic g -tensor affords a negative D value of about -20 cm^{-1} , which is in good agreement, considering the different experimental techniques, with that obtained in solution from the determination of the χ -tensor. Interpretation of the zero-field splitting parameter values is beyond the scope of this work. It can be noted, however, that negative values of D have also been observed in deoxymyoglobin¹⁶ and in other iron(II) compounds.⁴⁵

NMR studies of model porphyrin compounds suggest that the dipolar effects on chemical shift are generally small for the $S = 2$ state,¹⁹ indicating weak magnetic anisotropy in these compounds.^{25,53} However, in the ferroCyt c' , paramagnetic shifts of similar magnitude as in the ferriCyt c' were observed as evidence of a large magnetic susceptibility anisotropy in the reduced form. In comparison with myoglobin, the axial magnetic anisotropy in the ferroCyt c' is about 3 times larger than that in the deoxymyoglobin¹⁶ and comparable to low-spin iron(III) compounds.⁵¹ Moreover, the ferroCyt c' exhibits a nonnegligible rhombic anisotropy, as inferred from the NMR and susceptibility results.

Interestingly, the z -axis orientation of the magnetic susceptibility tensor does not coincide with the Fe–N imidazole direction, in contrast with high-spin iron(III) hemoproteins,²⁷ but is tilted about 30° toward the 5-meso proton. This direction is approximately perpendicular to the H122 imidazole plane, as determined by X-ray crystallography in both the oxidized and diamagnetic forms (Figure 8). Such a tilt has been also observed by NMR spectroscopy in sperm whale deoxymyoglobin.¹⁶ The location of the z -axis above the porphyrin plane cannot be unambiguously characterized in the latter case, as two solutions fit the data: the z -axis is either located in the imidazole plane with a negative ZFS axial parameter or perpendicular to the imidazole plane with a positive ZFS axial parameter.¹⁶ In horse deoxymyoglobin, where the electric field gradient (EFG) tensor and the magnetic tensor are aligned, a deviation of the principal axis of the EFG tensor from the heme normal has also been observed by Mössbauer spectroscopy.⁵⁴ As in sperm whale myoglobin, its orientation was not unambiguously determined; however, one of the solutions corresponds to a 40° tilt of the z -axis from the heme normal and a y -axis in the heme plane and approximately perpendicular to the imidazole plane. The tilt of the magnetic susceptibility tensor axis, observed not only in the ferroCyt c' but also in different myoglobins, seems to be a common feature of high-spin iron(II) hemoproteins. Explanation of such a shift from the usual 4-fold symmetry induced by the porphyrinic ligand is not straightforward, especially as the tilt occurs along other directions in myoglobins. The difference in the tilt direction could be, however, related to the counterrotation of the χ -tensor and the axial ligand described for the $S = 1/2$ hemoproteins.⁵⁵ On

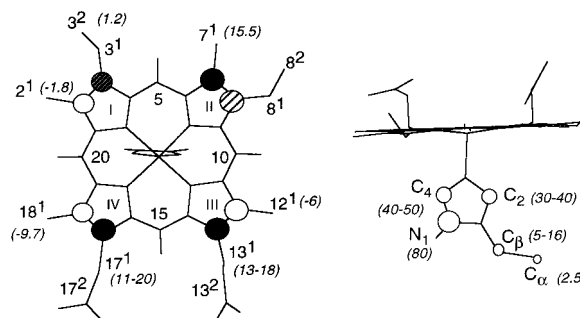


Figure 9. Electronic spin delocalization on the heme (left) and His122 (right) in the ferrocyclochrome c' of *Rb capsulatus*. The propionate groups point toward the front of the figure. Location of the imidazole ligand is the inverse in the Cyt c' with respect to myoglobins. Heme substituents were named following the IUPAC recommendations. Open and full circles on the pyrrolic positions correspond to positive and negative electronic spin density, respectively. Dashed circles correspond to spin delocalization inferred from symmetry. The estimated contact shifts are indicated in parentheses.

the other hand, this difference could be explained by an indetermination on the z -axis orientation in myoglobins or, as proposed from resonance Raman spectroscopy results, by a rotation of the histidinyll plane around the Fe–N bond between ferri- and ferroCyt c' .¹⁴ As the location of the tilt plane is either perpendicular or parallel to the histidinyll ring, the symmetry break could be due to an interaction between one of the d -orbitals of the iron and the π -orbital of the His ligand. In oxidized $[4\text{Fe-4S}]^{3+}$ iron–sulfur clusters, of (approximate) C_{2v} symmetry, the g -tensor principal z -axis is tilted by up to 20° from its expected location parallel to the C_2 molecular axis.⁵⁶ A phenomenological model taking into account d -orbital mixing has been proposed to interpret such an observation. An $\sim 10\%$ mixing, linked to symmetry lowering from the ideal C_{2v} one, turns out to be sufficient.⁵⁶ This implies that a slight shift from symmetry could result in large variations of the magnetic properties. Determination of the three-dimensional structure of a ferroCyt c' as well as of the magnetic susceptibility tensor orientation in other iron(II) hemoproteins is clearly needed to further investigate the exact origin of the tilt.

Contact Shifts of the Heme Protons. On the basis of the dipolar contribution, the contact shift contribution (and the orbitals involved in the spin density delocalization) can be determined. For His122, a large positive contact contribution is measured along the side chain (see Figure 9) (+80 ppm on the N1H and +10 ppm on the C^β). Such values are in agreement with the large contact shift expected from the interaction of the monopotential d_{z^2} orbital with the ligand and the σ -spin density delocalization.¹⁹

In hemic compounds, the lobes of the highest d -orbital (the $d_{x^2-y^2}$) are oriented toward the four nitrogens of the ring. Consequently, a single occupancy of this orbital must lead to positive spin density on the pyrrolic position through the σ -orbitals and results in large downfield shifts. This mechanism has been put forward to explain the large downfield shifts observed for pyrrolic or methyl protons in ferric high-spin models or proteins.¹⁹ In high-spin ferrous compounds, the $d_{x^2-y^2}$ orbital is also monopotential, and downfield shifts of pyrrolic protons in model complexes and methyl protons in hemoproteins have, indeed, been observed.¹⁹ Moreover, as shown in the sperm whale myoglobin, the contact shift values actually support a significant positive electron spin density on these positions (see Table 4), which has been ascribed to σ -spin delocalization.¹⁶

(53) Horrocks, W.; Greenberg, S. *Biochim. Biophys. Acta* **1973**, 322, 38–44.

(54) Kent, T.; Spartalian, K.; Lang, G.; Yonetani, T. *Biochim. Biophys. Acta* **1977**, 490, 331–340.

(55) Shokhirev, N. V.; Walker, F. A. *J. Am. Chem. Soc.* **1998**, 120, 981–990.

(56) Lepape, L.; Lamotte, B.; Mouesca, J.-M.; Rius, G. *J. Am. Chem. Soc.* **1997**, 119, 9757–9770.

In contrast, the electron spin delocalization in the ferrocyclochromes *c'* appears to be more complex. Whereas large downfield shifts are effectively found for some methyl positions, upfield shifts for other nuclei on the same pyrrolic ring are also observed. Moreover, the amplitude of the positive contact shift is twice as large as in deoxymyoglobin. The distribution of the spin density shows a 2-fold symmetry defined by a plane perpendicular or parallel to the imidazole plane and presents a pattern compatible with sign alternation along the heme position.

A first explanation would be that the spin density delocalization occurs only through interaction of the iron orbitals with π -orbitals of the porphyrin moiety. This however implies that the $d_{x^2-y^2}$ is either unoccupied or doubly occupied; both hypotheses can be excluded on the basis of the iron pentacoordination^{13–15} and the magnetic susceptibility and EPR data. An alternate explanation relies on two simultaneous spin density delocalizations: the expected σ -spin delocalization due to the monooccupation of the $d_{x^2-y^2}$ and a concomitant density occurring through the interaction of the ring π -orbitals and the d_{xz} and d_{yz} orbitals of the iron. The observed upfield shift would result from a larger negative spin density, which balances on the methyl carbons 2, 8, 12, and 18 the positive spin density observed in high-spin ferrous compounds such as deoxymyoglobin. From this point of view, it must be noted that the downfield shifts of the protons located on methyl carbon 7 and α -carbons of propionate 13 and 17 are larger here than in the deoxymyoglobin: a positive spin density probably adds up to those due to σ -spin delocalization. This leads us to propose a negative π -spin density on the 7, 13, and 17 pyrrolic positions when the 2, 8, 12, and 18 positions experience positive π -spin density, as illustrated in Figure 9. If this pattern holds true, the nature of the π -orbital implicated in the spin delocalization must be addressed. Indeed, the π -orbitals of the porphyrin ring, which are generally involved in spin delocalization, are either the filled $3e(\pi)$ or the empty $4e(\pi^*)$, owing to their symmetry properties.⁴³ The spin density distribution of these orbitals is, however, inconsistent with the pattern deduced from the observed contact shift, i.e., alternate signs on the same pyrrolic unit. Molecular orbital calculations are presently underway to understand the mechanism involved in the spin delocalization.

Contrary to other high-spin ferrous proteins or model compounds, and in particular to deoxymyoglobin, Cyt *c'* exhibits a high magnetic susceptibility anisotropy, leading to large dipolar shifts, a different orientation of the magnetic susceptibility tensor, and an original scheme of spin density delocalization. Although these differences remain to be explained, the different orientation of the His ring with respect to the heme is a striking

feature. For deoxymyoglobin, the imidazole plane eclipses two Fe–N(pyrrole) bonds⁵² as in the model of myoglobin [$\text{Fe}^{\text{III}}(\text{OEP})(2\text{-MeHim})$]⁺⁵⁷ in a position thermodynamically the most favorable.⁵⁸ In the Cyt *c'*, the imidazole plane nearly bisects the Fe–N pyrrole bonds,⁴ a thermodynamically unfavorable position probably strained by the covalent links between the polypeptidic chain and the heme. In the same way, the structure of the deoxymyoglobin of *Aplysia limacina*⁵⁹ indicates a nearly similar position of the imidazole plane to the Cyt *c'*, while the pattern of the methyl resonances is also similar to that of Cyt *c'*.⁶⁰ It could be speculated that these structural constraints lead to perturbations of the symmetry around the iron which, in turn, allow unusual mixing of orbitals. From this point of view, it must be noted that the (OETPP)(Fe)Cl, which displays important distortion of the macrocycle due to steric constraints, shows magnetic properties similar to those of ferriCyt *c'*.⁶¹

Acknowledgment. We thank Dr. Martin Blackledge for critical reading of the manuscript and Dr. Jean-Marie Mouesca and Dr. Catherine Bougault for helpful discussions. This work has been supported by the Centre National de la Recherche Scientifique, the Commissariat à l'Énergie Atomique, Molecular Simulations Inc., and NIH Grant GM21277. This is publication no. 545 of the Institut de Biologie Structurale "Jean Pierre Ebel". P.T. was a recipient of a CEA fellowship.

Note Added in Proof. To convert to SI units (m^3/mol) the magnetic anisotropy, the values must be multiplied by $4\pi N_a$ ($N_a = 6.02 \times 10^{23}$).

Supporting Information Available: One table (assignments for the ^1H and ^{15}N chemical shifts of *Rb. capsulatus* ferrocyclochromes *c'*) and one figure (EPR spectra at 4.2 K) (PDF). This information is available free of charge via the Internet at <http://pubs.acs.org>.

JA9820745

(57) Scheidt, W. R.; Geiger, D. K.; Lee, Y. J.; Reed, C. A.; Lang, G. J. *Am. Chem. Soc.* **1985**, *107*, 5693–5699.

(58) Scheidt, W. R.; Chipman, D. M. *J. Am. Chem. Soc.* **1986**, *108*, 1163–1167. Scheidt, W. R.; Osvath, S. R.; Lee, Y. J. *J. Am. Chem. Soc.* **1987**, *109*, 1958–1953.

(59) Bolognesi, M.; Onesti, S.; Gatti, G.; Coda, A.; Ascenzi, P.; Brunori, M. *J. Mol. Biol.* **1985**, *205*, 529–544.

(60) Wüthrich, K.; Hochmann, J.; Keller, R. M.; Wagner, G.; Brunori, M.; Giacometti, C. *J. Magn. Reson.* **1975**, *19*, 111–113.

(61) Cheng, R.-J.; Chen, P.-Y.; Gau, P.-R.; Chen, C.-C.; Peng, S.-M. *J. Am. Chem. Soc.* **1997**, *119*, 2563–2569.

(62) Bersch, B.; Brutscher, B.; Meyer, T. E.; Marion, D. *Eur. J. Biochem.* **1995**, *227*, 249–260.